scientific reports

Check for updates

OPEN

A reduction in energy costs induces integrated states of brain dynamics

Kosuke Takagi

In the human brain, interactions between multiple regions organize stable dynamics that enable enhanced cognitive processes. However, it is unclear how collective activities in the brain network can generate stable states while preserving unity across the whole brain scale under successive environmental changes. Herein, a network model was introduced in which network connections were adjusted to reduce the energy consumption level by avoiding excess changes in the activated states of each region during successive interactions. For time series data obtained from fMRI images, a connection matrix was generated by a simulation, and the predictions made by this matrix yielded accurate results relative to the real data. In this simulation, the adjustment process was activity-dependent, in which the interregional connections between intense active regions were reinforced to prohibit free behaviours. This resulted in a reduced excess energy loss and the integration of multiple regional activities into integrated dynamic states under constraints imposed by other regions. It was suggested that the simple rule of saving excess energy costs plays an important role in the mechanism that regulates large-scale brain networks and dynamics.

In the human brain, cognitive processes associated with consciousness arise from the collective activities of neurons[1]. Stimuli derived from inner and outer environments evoke signal processing activities in multiple brain regions[2,3]. Such activities are organized into synchronized dynamic states across the whole brain and enable the vast functionality of the human brain, thus ensuring flexible adaptation and facilitating complex cognition[4,5]. These activities preserve a unified state during reactions to stimuli and maintain stability or metastability[6,7]. This stability enables enhanced cognition and supports our mental experiences in real life, which are continuous and stable[8–11]. These dynamics are based on the brain network, which regulates the interactions between neurons and multiple brain regions by adjusting their connectivity[12–15]. However, it is unclear how the brain generates such a network structure that can preserve stable dynamic states.

The correlations among brain regions are depicted by functional and structural connectivity mechanisms, which are derived from the activity patterns and anatomical structures, respectively, observed from imaging devices such as fMRI[16,17]. Connectivity analyses have revealed the network features that constitute hierarchical structures composed of stable core regions and specialized modules[18,19]. In a hierarchical structure, a stable group of core functional regions works to adjust regional activities and stabilize the system[20–23]. These controlled behaviours occurring across multiple regions induce coherent patterns and result in strong correlations between regions. These integrated states supported by strong connectivity are thought to form the basis of consciousness that emerges with a continuous stream of mental experiences[24,25]. In fact, the strength of interregional connectivity is an indicator of consciousness, which decreases in lower consciousness states such as that induced by anaesthesia[26–28]. However, the mechanisms that form the hierarchical brain network underlying organized dynamic states are not clearly understood[29–31].

The brain is an organ that requires enormous amounts of energy to maintain its activity. Across various species, higher brain energy demands are considered to be associated with greater cognitive capabilities[32]. On the other hand, limited energy resources work as constraints imposed on activity and network formation in the brains of individuals[33]. According to research evidence, energy constraints affect neuronal activity and synaptic plasticity at the cellular and synaptic levels[34,35]. This results in a cost premium and an efficient large-scale network structure, which can be characterized by features akin to those of small-world networks[36–40]. In this paper, it was assumed that a reduction in the degree of excess energy loss had a large impact on the formation of a large-scale brain network[41–43].

Results

Stability of regional brain activity

To reduce the energy consumption level, the developed model was assumed to stabilize brain activity by reducing the energy loss induced during signal processing. By using fMRI data, the activity level of a region could be

Independent Researcher, Saitama, Japan. email: coutakagi@gmail.com

estimated by the time series of the signal intensities $s(i, t)$ observed for region i at time t. In the energy saving model, activity state fluctuations were expected to be reduced, and the following term was minimized:

$$\partial_t s^2(i,t). \tag{1}$$

In this model, regional activity was adjusted to prevent rapid changes and achieve stable energy states in each region. In an extreme case without stimuli derived from inner and outer environments, this model yields the static state, in which the signal of each region is set to a constant value, i.e., the mean value of the region. However, for adaptive systems that receive successive stimuli from these sources, decreasing activity time variations and gradual time changes, as shown in Fig. 1c, are expected.

Empirical evidence suggested the existence of an energy saving mechanism based on the time series data of the activity signals. First, for regions parcellated using a brain atlas (Fig. 1a), the series data were extracted from fMRI datasets as the mean intensities of different regions. These regions composed subnetworks such as the default mode and visual networks between strongly connected regions (Fig. 1b). The extracted signals were preprocessed by subtracting the mean value of each region (Fig. 1c). Thus, they represent the relative differences, i.e., increases and decreases, of the activity level for each region from the mean value.

Then, the mean absolute values of the signal time differences, $s(i,t+1)-s(i,t)$ and $s^2(i,t+1)-s^2(i,t)$, were evaluated and compared to randomly reordered series data (Fig. 1d). These values were normalized by dividing them by those of randomized data. The estimated values smaller than 1, which were the expected values for the randomly reordered case, indicated that the activity pattern transitions were controlled to suppress disorganized and rapid changes. Because signal amplitude fluctuations are indicators of energy consumption[40], these findings might indicate that brain dynamics are involved in reducing energy consumption.

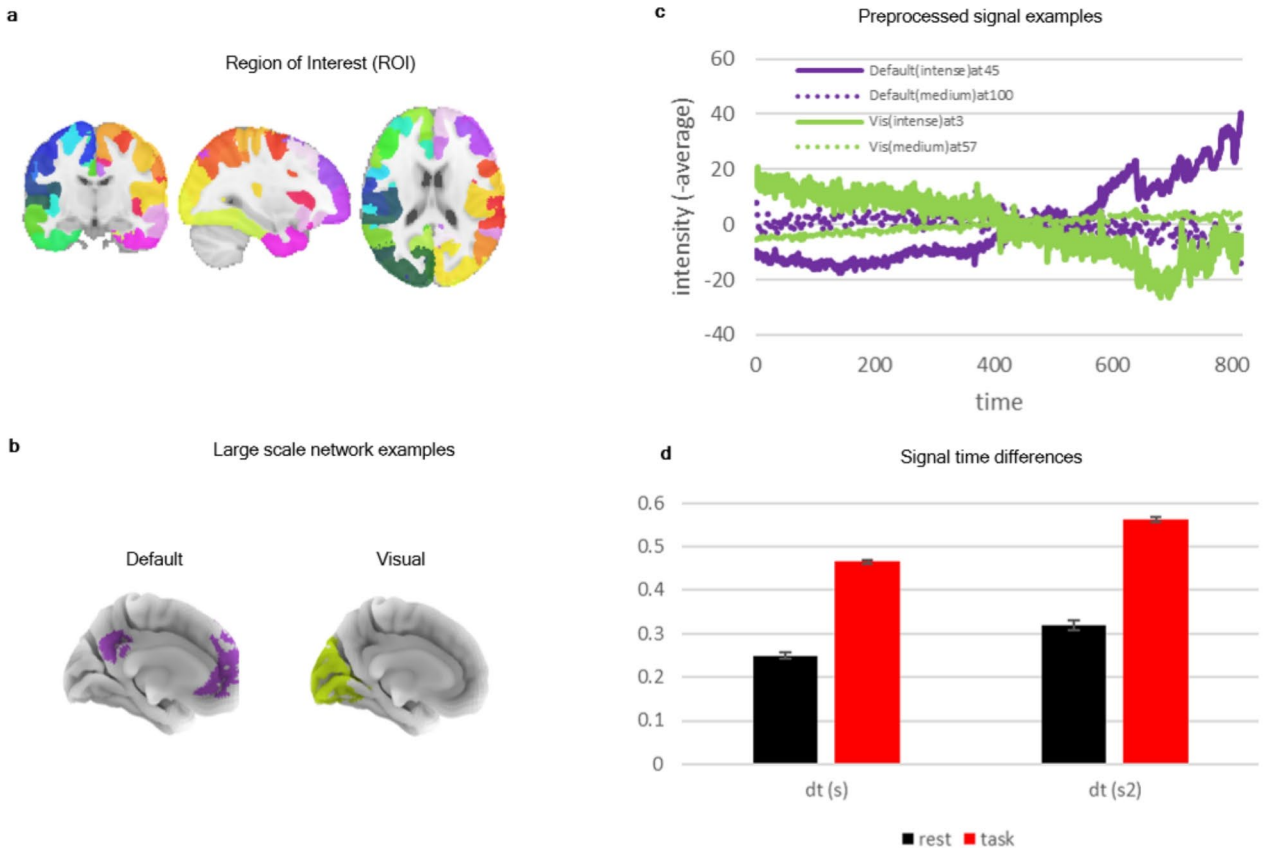

Fig. 1. Brain dynamics and stability. (**a**) Parcellations. Parcellations based on a brain atlas with 100 parcels, which divided the large-scale brain regions into subregions, are visualized based on frontal, axial, and lateral cuts. (**b**) Examples of large-scale networks. Surface plots of large-scale network examples, such as the default mode network and visual network, are shown. (**c**) Preprocessing. Examples of the preprocessed signals are shown. The time series data of two regions extracted from the default mode are displayed with purple lines, and the visual subnetworks are shown with green lines. In these plots, the raw signals of the resting-state fMRI data were normalized by subtracting the mean value of each region. (**d**) Time differences and stability. The time differences of the signals s and s^2 were estimated and normalized by the randomly ordered data. The time differences $dt(s) = s(i,t+1) - s(i,t)$ and $dt(s^2) = s^2(i,t+1) - s^2(i,t)$ for each time and each region, respectively, were taken and divided by the differences produced by the randomly ordered data. Then, the mean absolute values were calculated and are shown along with the standard errors.

Energy saving and connection adjustments

To clarify the effect of the energy saving mechanism on network formation, a simulation was conducted on the given sets of signals obtained from fMRI images, as above. First, the definition of the state transitions of activities was given based on the connection matrix $c(i, j)$ between pairs of regions i and j as

$$s(i, t+1) = \Sigma c(i, j) s(j, t) \tag{2}$$

in the general descriptions. Through these connections, regions interact with exciting or inhibiting activities on other sides according to the positive or negative values of the terms on the right-hand side of this equation. Then, substituting this definition into Eq. (1) led to the relation

$$\partial_t s^2(i, t) \simeq 2s(i, t+1)(s(i, t+1) - s(i, t)) \simeq 2(\Sigma c(i, j) s(j, t))(\Sigma c(i, j) s(j, t) - s(i, t)). \tag{3}$$

Under the assumption of energy savings, the connection $c(i, j)$ was refined to minimize Eq. (3) in this model.

In the simulation conducted using a machine learning method, the connection matrix was trained to reduce the energy loss defined as Eq. (3) for the given set of signals $s(i, t)$. Then, predictions for the succeeding states were made by multiplying the obtained connection matrix according to Eq. (2). In Fig. 2a, the predictions given by this model were plotted against the real observation data. Compared to those made by the functional connectivity (FC) and the random matrix in the same manner, the predictions of the proposed model were plotted almost as straight lines, demonstrating their accuracy. In Fig. 2b, the accuracy of these predictions were numerically estimated by their correlations using the Pearson correlation coefficient, where the results obtained for the resting state exhibited highly accurate values exceeding 0.9. The same result was obtained for the task cases, which maintained values above 0.7. The results showed that the proposed method can be applied equally to cases under resting-state and task conditions.

Stability and connection adjustments

The correlations between the adjusted connections and regional activities provided detailed descriptions of the mechanisms that stabilized the dynamics of the brain network. According to the minimization of the energy term, Eq. (3) was used to refine the connection strengths in an activity-dependent manner. Due to this condition, the internal signal states $s(i, t)$ and the total input obtained from the outer regions $\Sigma c(i, j) s(j, t)$ were balanced: $(\Sigma c(i, j) s(j, t) - s(i, t)) \simeq 0$. According to this condition, the connections to region i were strengthened when

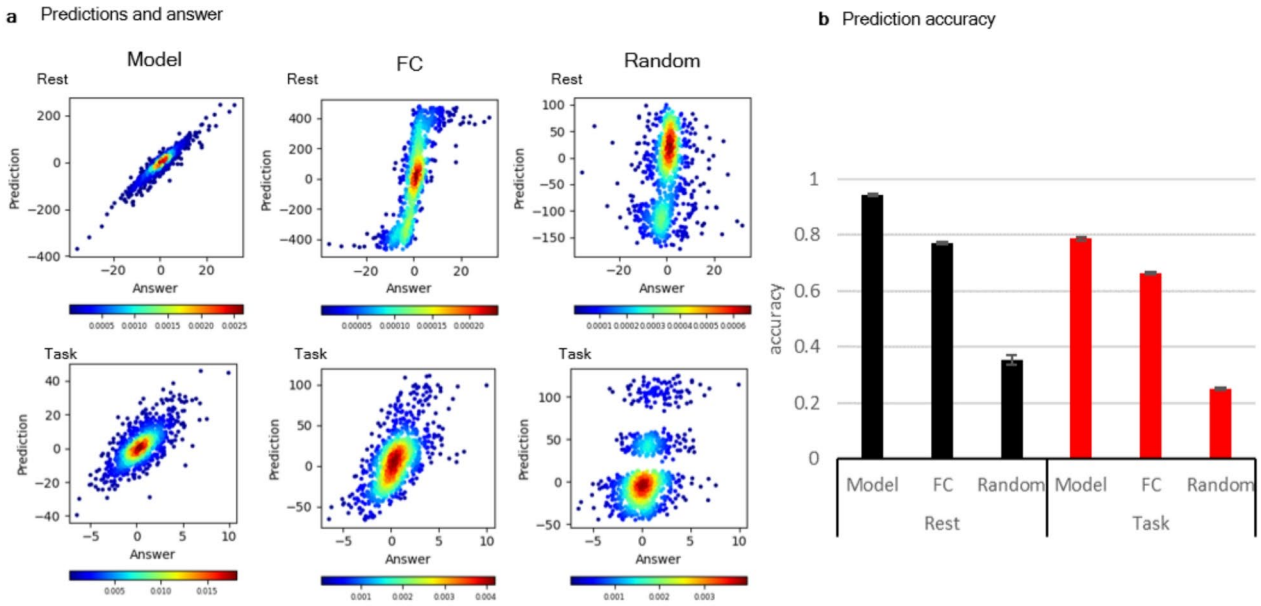

Fig. 2. Model prediction accuracy. (**a**) Predictions and answers. The predictions are shown on the scatter plot, with the answers on the horizontal axis and the predictions on the vertical axis, where colours indicate the density of each plot. The predictions were made by multiplying the connection matrices by the set of signals $s(i, t)$ and compared against the answers, i.e., the signals at $t + 1$, $s(i, t + 1)$. The plots were made with the matrix of the model (Model), the functional connectivity (FC), and the random matrix (Random). For each scatter panel, 1000 points randomly selected from whole datasets for each case (resting or task completion) were plotted. (**b**) Mean prediction accuracy. The prediction accuracy achieved for each fMRI image was evaluated by the correlation coefficient. Then, the mean accuracy of the model predictions made for 100 resting-state images and 699 task fMR images were compared to the functional connectivity (FC) and random matrix (Random) predictions with standard error bars.

the amplitude of signal $s(i, t)$ was large. The correlation plot in Fig. 3a shows that active regions with large amplitudes and large absolute intensity values acquired strong connections during the model training process.

These strengthened connections in the active regions stabilized the activity in these regions. The plot in Fig. 3b shows the correlation between the amplitude and the signal time differences. They had an inverse correlation, and the active regions had small temporal differences, indicating stability. In this network, the active regions were strongly constrained by other regions (Fig. 3a) and prohibited from behaving freely (Fig. 3b). This could be directly confirmed by the accuracy of the prediction obtained for each region relative to the time differences (Fig. 3c). Thus, the results showed that the activity flows in intense active regions strictly followed the relation described by Eq. (2). These regions contrasted with the inactive regions possessing small amplitudes, which behaved freely under loose connections and had relatively low prediction accuracies. In summary, the model provided a simple picture of the network formation process. According to this mechanism, active regions acquired strong connections and stabilized their activities under the strong constraints imposed by other regions.

As a consequence, the dynamics of the network resulted in organized states. The correlation plot in Fig. 4a indicates the inverse relations between the stability of the network, the time difference of each region, and the functional connectivity level, which are the interregional correlations in the time series data. The stable regions comprised subnetworks, which exhibited strong functional connectivity, as shown in Fig. 4b. The communities consisting of stable and active regions, which were located on the left side of this plot (Fig. 4b), had synchronized activities with higher connectivity values among their community members. These results are summarized in Fig. 4c.

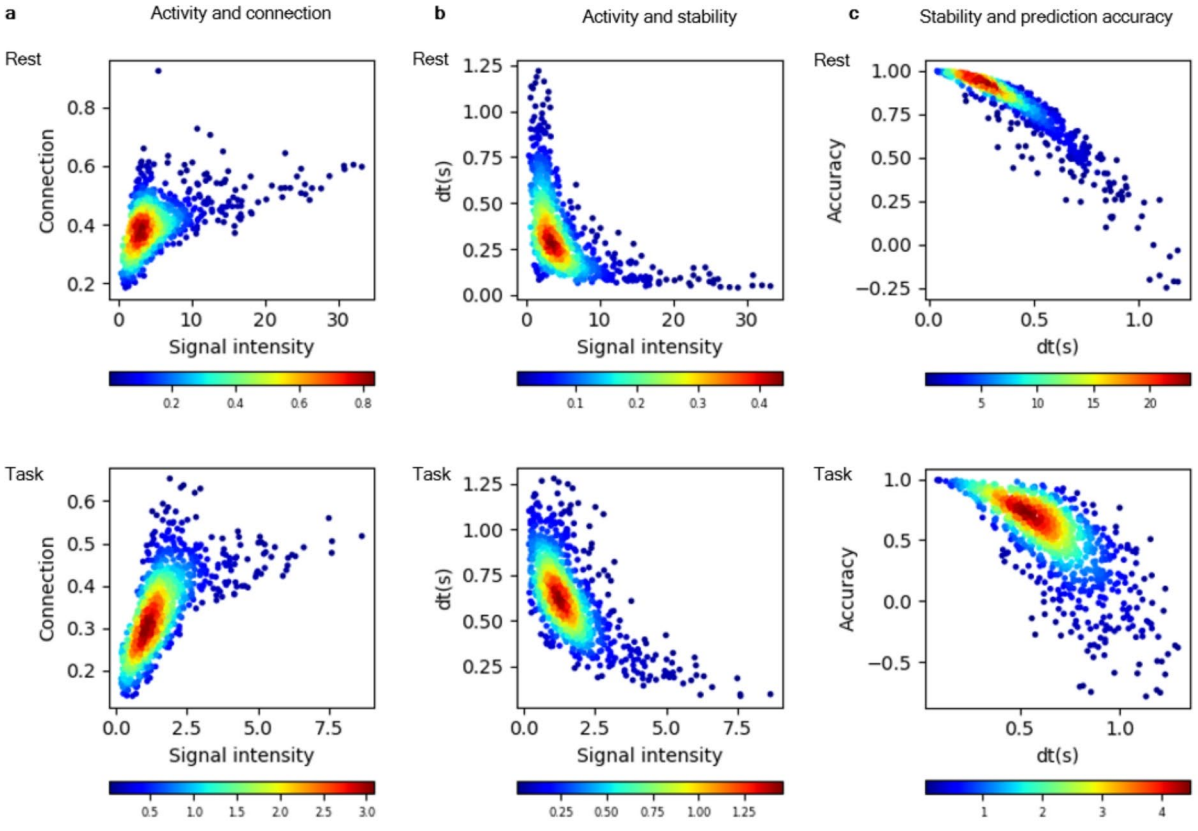

Fig. 3. Model network formation. (**a**) Activity and connection strength. For the horizontal axis, the activity level was estimated by the absolute values of the signal intensities. Then, the mean time series values were plotted against the connection strengths, i.e., the mean absolute values of the network connections exhibited by each region, on the vertical axis. The density map was made in the same manner as those presented in the previous figures. (**b**) Activity and stability. The activity level, which was the same as that in plot (a), was plotted on the horizontal axis and compared to the signal time differences that were calculated as in the case of Fig. 1d on the vertical axis. During each calculation, the mean absolute value was taken. (**c**) Stability and prediction accuracy. The time differences, represented by the values on the vertical axis of (**b**), were compared to the prediction accuracy of each region, which was calculated by the correlation coefficient between the predictions and answers produced for each region. These results were obtained in the same manner as those in the previous cases, as shown in Fig. 2a.

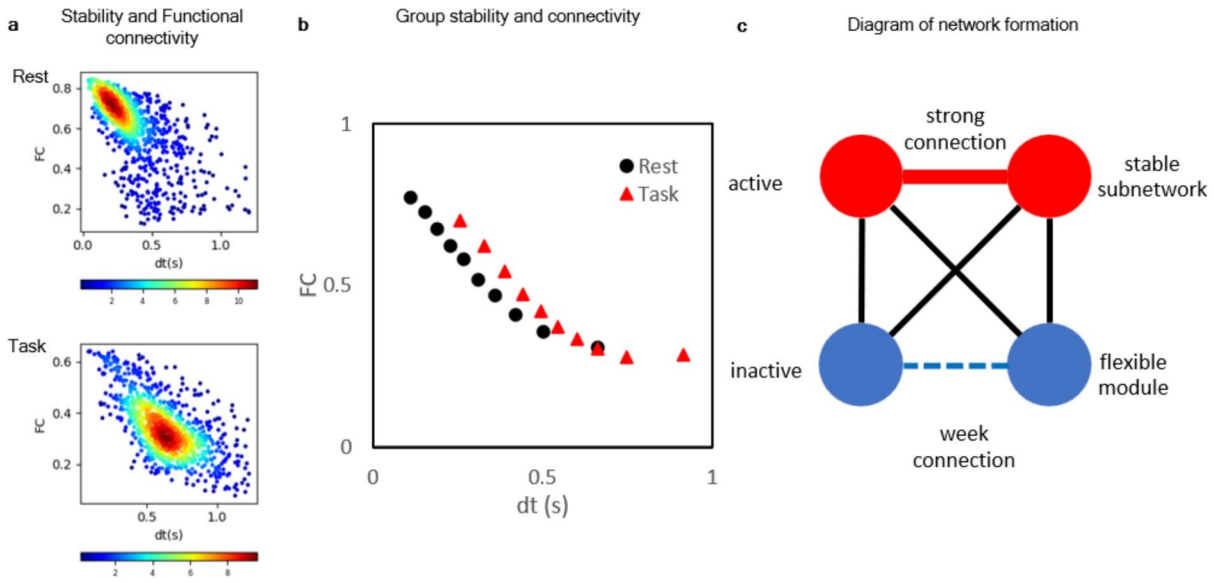

Fig. 4. Stability and functional connectivity. (**a**) Stability and functional connectivity. The mean absolute values of the functional connectivity for each region were plotted on the vertical axis against the time differences on the horizontal axis, and the values are given in Fig. 3b,c. The density maps were constructed in the same manner as those presented in previous figures. (**b**) Group stability and connectivity. The relationships between the regional stability levels and functional connectivity strengths are summarized in this plot. The plots of single regions in panel (**a**) are grouped and averaged. The 100 regions of each fMRI image dataset were classified into 10 groups according to their stability strengths, and the time differences of the signals are given on the horizontal axes in (**a**). Then, the internal connectivity was evaluated by averaging only the functional connectivity between the regions sharing the same group. Then, they were plotted and overlaid with the rest cases (the black circles) and the task cases (the red triangles). (**c**) Network formation diagram. This illustration summarizes the network formation process of this model. As shown in Fig. 3a, the active regions with intense signals, illustrated as red circles, acquired strong connections, which are represented by thick red lines between the circles, and comprised subnetworks, as shown in (**b**). On the other hand, inactive regions, illustrated as blue circles, had weak connections, which are illustrated by blue dashed lines, and might have behaved freely as flexible modules. The connections between active and inactive regions had medium strengths, as illustrated by black lines, compared to those of other connections.

Discussion

In summary, it was shown that the energy saving mechanism induced a hierarchical network structure that was dependent on the activity level of each region, as displayed in Fig. 4c. According to this mechanism, the active states $s(i, t)$ and the total input obtained through interregional connections $\Sigma c(i, j)s(j, t)$, were balanced. Then, active regions with strong signal amplitudes tended to acquire strengthened connections (Fig. 3a). Due to this activity-dependent adjustment process, mutual effects resulted in strengthened selective connections between intense active regions, and they formed a community with strong inter-region connectivity (Fig. 4b). These regions contrasted with the inactive regions, which had loose connections. The connections between these inactive modules were weakened, and they might have composed independent modules in the global network, which enabled them to respond freely to changing environments. While the connections between the active and inactive regions conserved intermediate strength, the inactive regions were affected by stable core networks. Thus, this mechanism might have induced hierarchical relationships with the core networks and modules[12,18], where the activities occurring in the stable core networks were more dominant than those of the modules[10].

Additionally, according to this mechanism, the integrated states across the whole brain emerged spontaneously with reinforced connections, which restricted activities with mutual constraints between regions. When the terms in Eqs. (1) and (3) were minimized, each region was prohibited from behaving freely and was required to follow the transition rules $s(i, t + 1) = \Sigma c(i, j)s(j, t)$ shown in Eq. (2). Therefore, the regional activities could not be separated from each other, and the brain dynamics were organized into integrated states. In addition, because this constraint imposed by the connection matrix might have preserved the causal relationships between transition patterns, the information loss may also have been reduced[38,41,42].

Thus, as discussed above, the energy saving mechanism introduced in this study provides a possible basis for the origin of some brain dynamics features, such as stability and activity integration. This mechanism induces the formation of subnetwork communities by reinforcing the connections between active regions, while it allows inactive regions to exhibit relatively free behaviours in response to temporal changes. This hierarchical structure contributes to saving energy by stabilizing the active regions, which consume more energy, and distributing

temporal processing tasks to independent modules, which consume less energy. As a consequence, dynamics preserve integrated states by allowing flexible responses to environmental changes. These features support consciousness, which is continuous and consistent, and an explanation of these origins is given from a unified perspective.

In fact, evidence supporting this model can be found in empirical results. In this model, the assumption concerning energy savings demands that the time fluctuations from the mean values are controlled to be small. On the other hand, cognitive phenomena such as change blindness, the failure to notice large changes in an object or scene, are known. Experiments on this phenomenon have shown that visual perceptions are continuously smoothed over time[11]. In both cases, the small fluctuations tend to be neglected, and the signals are reduced to their stable mean state. Although a further investigation is needed to clarify these relationships, mechanisms similar to energy savings might affect perceptions and support stable cognitive functioning in our daily experience.

However, issues and limitations remain with respect to the mathematical formulation of this model. It provides an approximation, and in fact, the prediction accuracy, especially that attained in task-evoked cases, is lower than that achieved in the resting state cases, as shown in Fig. 2b. Factors such as the time dependency of variables and the variability of mean value constants influence the formula, resulting in the emergence of additional terms in Eq. (3). Thus, the formulation of this model remains an approximation, and an extension is needed to obtain more accurate predictions in the future.

Methods

fMRI datasets

fMRI image datasets were downloaded from the OpenNeuro database, which is a publicly available database for sharing brain images, with accession number ds000224[44,45]. Each dataset contained 100 fMRI data points for 10 individuals with 10 resting-state stations and 70 images for 10 individuals with 7 sessions involving 5 different tasks. Then, 100 resting-state *fMR* images and 699 task fMR images were used in this study.

Preprocessing and parcellation

To handle and preprocess the fMRI images, Nilearn[46], a python library for neuroinformatics, was used. Then, activity signal time series were extracted for 100 cortical regions of interest that were parcellated by using the Schaefer atlas[47]. In Fig. 1a, the Montreal Neurological Institute template (MNI-152)[48] was used for the overlayed background image. FreeSurfer[49], which could be obtained from Nilearn, was also employed. Additionally, Yeo 7-networks[50] were used for displaying the examples of large-scale networks, as shown in Fig. 1b. For each region, the time series of the fMRI signals were normalized by subtracting the mean value of each region (Fig. 1c). In this figure, the plotted regions were selected according to the mean amplitude values. Thus, regions with large amplitudes and those with intermediate amplitudes are contrasted in this figure. These normalized signals were used for all the analyses conducted in this study.

Simulation

According to the energy saving assumption, the network model adjusted connection $c(i, j)$ to minimize Eq. (3). In this simulation, TensorFlow[51], a python package for machine learning, was used. The connection matrix was learned to minimize the above term as the objective function for a given set of time series data for each fMR image; these data were randomly split into training and validation groups at ratios of 0.9 and 0.1, respectively. During this learning process, the Adam optimizer[52] was used, and training was repeated 3000 times. For each calculation step, the signal sets were divided by the standard deviation to prevent divergence.

Unlike the typical deep learning models that are composed of multiple layers, this model has a simple structure with a single connection matrix. To demonstrate the robustness of the training system, different parameter sets were tested. For example, setting the ratios of the training groups to 0.9 and 0.8 yielded almost the same prediction accuracy as that of the results given in Fig. 2b, where the mean accuracies attained for the resting state were 0.945 and 0.944, respectively, and they were 0.786 and 0.785, respectively, for the task cases.

Predictions

The predictions in Figs. 2 and 3 were made with the generated matrices $c(i, j)$, which were obtained as described above. For each time t, the successive signal state was calculated by multiplication according to Eq. (2). Then, the results were compared to the real observed data for $s(i, t + 1)$ in Fig. 2. In these figures, the predictions were compared to those yielded by other matrix sets, the functional connectivity and the random matrix. The functional connectivity was calculated by the Pearson correlation coefficients between different regions, where the raw signals are used without subtracting the mean values, and each connection $c(i, j)$ was substituted by this value. The random matrix was formed by random values taken from the range $[1, -1]$.

Statistics

For the calculation of the Pearson correlation coefficient, the SciPy python package[53] was used.

Data availability

The fMRI image data were downloaded from OpenNeuro (https://openneuro.org/datasets/ds000224/versions/1.0.3).

Code availability

The Python scripts for the developed model are available on GitHub (https://github.com/coutakagi/2024v1/).

Received: 18 June 2024; Accepted: 26 March 2025
Published online: 03 April 2025

References

1. Koch, C., Massimini, M., Boly, M. & Tononi, G. Neural correlates of consciousness: Progress and problems. *Nat. Rev. Neurosci.* **17**, 307–321 (2016).
2. Kriegeskorte, N., Goebel, R. & Bandettini, P. Information-based functional brain mapping. *PNAS* **103**, 3863–3868 (2006).
3. Yarkoni, T., Poldrack, R., Nichols, T. & Van Essen, D. Large-scale automated synthesis of human functional neuroimaging data. *Nat. Methods* **8**, 665–670 (2011).
4. Rodriguez, E., George, N., Lachaux, J. & Martinerie, J. Perception's shadow: Long-distance synchronization of human brain activity. *Nature* **397**, 430–433 (1999).
5. Varela, F., Lachaux, J., Rodriguez, E. & Martinerie, J. The brainweb: Phase synchronization and large-scale integration. *Nat. Rev. Neurosci.* **2**, 229–239 (2001).
6. Deco, G., Kringelbach, M., Jirsa, V. & Ritter, P. The dynamics of resting fluctuations in the brain: Metastability and its dynamical cortical core. *Sci. Rep.* **7**, 3095 (2017).
7. Shine, J. et al. Human cognition involves the dynamic integration of neural activity and neuromodulatory systems. *Nat. Neurosci.* **22**, 289–296 (2019).
8. Baldassano, C. et al. Discovering event structure in continuous narrative perception and memory. *Neuron* **95**, 709–721 (2017).
9. Luppi, A. et al. Consciousness-specific dynamic interactions of brain integration and functional diversity. *Nat. Commun.* **10**, 4616 (2019).
10. Mashour, G., Roelfsema, P., Changeux, J. & Dehaene, S. Conscious processing and the global neuronal workspace hypothesis. *Neuron* **105**, 776–798 (2020).
11. Manassi, M. & Whitney, D. Illusion of visual stability through active perceptual serial dependence. *Sci. Adv.* **8**, 2 (2022).
12. Park, H. & Friston, K. Structural and functional brain networks: From connections to cognition. *Science* **342**, 6158 (2013).
13. Bassett, D., Wymbs, M., Porter, M. & Grafton, S. Dynamic reconfiguration of human brain networks during learning. *PNAS* **108**, 7641–7646 (2011).
14. Gordon, E., Laumann, T., Gilmore, A. & Newbold, D. Precision functional mapping of individual human brains. *Neuron* **95**, 791-807.e7 (2017).
15. Gratton, C. et al. Functional brain networks are dominated by stable group and individual factors, not cognitive or daily variations. *Neuron* **98**, 439–452 (2018).
16. Honey, C., Kotter, R., Breakspear, M. & Sporns, O. Network structure of cerebral cortex shapes functional connectivity on multiple time scales. *PNAS* **104**, 10240–10245 (2007).
17. Bassett, D. & Sporns, O. Network neuroscience. *Nat. Neurosci.* **20**, 353–364 (2017).
18. Bullmore, E. & Sporns, O. Complex brain networks: Graph theoretical analysis of structural and functional systems. *Nat. Rev. Neurosci.* **10**, 186–198 (2009).
19. Bassett, D. & Bullmore, E. Small-world brain networks. *The Neuroscientist* **12**, 512–523 (2006).
20. Dosenbach, N. et al. Distinct brain networks for adaptive and stable task control in humans. *PNAS* **104**, 11073–11078 (2007).
21. Buckner, R. et al. Cortical hubs revealed by intrinsic functional connectivity: Mapping, assessment of stability, and relation to Alzheimer's disease. *J. Neurosci.* **29**, 1860–1873 (2009).
22. van den Heuvel, M. & Sporns, O. Network hubs in the human brain. *Trends Cogn. Sci.* **17**, 683–696 (2013).
23. Gilbert, C. & Li, W. Top-down influences on visual processing. *Nat. Rev. Neurosci.* **14**, 350–363 (2016).
24. Tononi, G., Boly, M., Massimini, M. & Koch, C. Integrated information theory: From consciousness to its physical substrate. *Nat. Rev. Neurosci.* **17**, 450–461 (2016).
25. Shine, J. et al. The dynamics of functional brain networks: Integrated network states during cognitive task performance. *Neuron* **92**, 544–554 (2016).
26. Vanhaudenhuyse, A. et al. Default network connectivity reflects the level of consciousness in non-communicative brain-damaged patients. *Brain* **133**, 161–171 (2010).
27. Boly, M., Moran, R., Murphy, M. & Boveroux, P. Connectivity changes underlying spectral eeg changes during propofol-induced loss of consciousness. *J. Neurosci.* **32**(20), 7082–7090 (2012).
28. Barttfeld, P. et al. Signature of consciousness in the dynamics of resting-state brain activity. *PNAS* **112**, 887–892 (2015).
29. Martin, S., Grimwood, P. & Morris, R. Synaptic plasticity and memory: an evaluation of the hypothesis. *Annu. Rev. Neurosci.* **23**, 649–711 (2000).
30. Neves, G., Cooke, S. & Blis, T. Synaptic plasticity, memory and the hippocampus: A neural network approach to causality. *Nat. Rev. Neurosci.* **9**, 65–75 (2008).
31. Magee, J. & Grienberger, C. Synaptic plasticity forms and functions. *Annu. Rev. Neurosci.* **43**, 95–117 (2020).
32. Magistretti, P. & Allaman, I. A cellular perspective on brain energy metabolism and functional imaging. *Neuron* **86**, 883–901 (2015).
33. Harris, J., Jolivet, R. & Attwell, D. Synaptic energy use and supply. *Neuron* **75**, 762–777 (2015).
34. Laughlin, S. Energy as a constraint on the coding and processing of sensory information. *Curr. Opin. Neurobiol.* **11**, 475–480 (2001).
35. Turrigiano, G. & Nelson, S. Homeostatic plasticity in the developing nervous system. *Nat. Rev. Neurosci.* **5**, 97–107 (2004).
36. Bassett, D. & Bullmore, E. Small-world brain networks. *The Neuroscientist* **12**, 512–523 (2006).
37. Achard, S. & Bullmore, E. Efficiency and cost of economical brain functional networks. *PLoS Comp. Biol.* **3**, e17 (2006).
38. Friston, K. The free-energy principle: A unified brain theory?. *Nat. Rev. Neurosci.* **11**, 127–138 (2010).
39. Bullmore, E. & Sporns, O. The economy of brain network organization. *Nat. Rev. Neurosci.* **13**, 336–349 (2012).
40. Tomasi, D., Wang, G. & Volkow, N. Energetic cost of brain functional connectivity. *PNAS* **110**, 13642–13647 (2013).
41. Takagi, K. Information-based principle induces small-world topology and self-organized criticality in a large scale brain network. *Front. Comput. Neurosci.* **12**, 65 (2018).
42. Takagi, K. Principles of mutual information maximization and energy minimization affect the activation patterns of large scale networks in the brain. *Front. Comput. Neurosci.* **13**, 86 (2020).
43. Takagi, K. Energy constraints on brain network formation. *Sci. Rep.* **11**, 11745 (2021).
44. Gordon, E. et al. Precision functional mapping of individual human brains. *Neuron* **95**, 791–807 (2017).
45. The midnight scan club (msc) dataset. https://openneuro.org/datasets/ds000224/versions/1.0.3. Online; Accessed 19-Aug-2021.
46. Nilearn. https://nilearn.github.io/stable/index.html. Online; accessed 19-Aug-2021.
47. Schaefer, A. et al. Local-global parcellation of the human cerebral cortex from intrinsic functional connectivity mri. *Cereb. Cortex* **28**, 3095–3114 (2018).
48. Fonov, V. et al. Unbiased average age-appropriate atlases for pediatric studies. *Neuroimage* **54**, 313–327 (2011).
49. Fischl, B. Freesurfer. *Neuroimage* **62**, 774–781 (2012).
50. Yeo, B., Krienen, F., Sepulcre, J., Sabuncu, M. & Lashkari, D. The organization of the human cerebral cortex estimated by intrinsic functional connectivity. *J. Neurophysiol.* **106**, 1125–1165 (2011).
51. Tensorflow. https://www.tensorflow.org/. Online; Accessed 19-Aug-2021.

52. Kingma, D. & Ba, J. *Adam: A method for stochastic optimization*. *arXiv preprint* arXiv:1412.6980 (2014).
53. Scipy. https://scipy.org/. Online; Accessed 19-Aug-2021.

Author contributions
KT designed the study, conducted the simulations and data analyses, and wrote the manuscript.

Funding
The author received no specific funding for this work.

Declarations

Competing interests
The author declares no competing interests.

Additional information
Correspondence and requests for materials should be addressed to K.T.

Reprints and permissions information is available at www.nature.com/reprints.

Publisher's note Springer Nature remains neutral with regard to jurisdictional claims in published maps and institutional affiliations.